NANO LETTERS

pubs.acs.org/NanoLett Letter

Gate-Tunable Proximity Effects in Graphene on Layered Magnetic Insulators

Chun-Chih Tseng, Tiancheng Song, Qianni Jiang, Zhong Lin, Chong Wang, Jaehyun Suh, Kenji Watanabe, Takashi Taniguchi, Michael A. McGuire, Di Xiao, Jiun-Haw Chu, David H. Cobden, Xiaodong Xu, and Matthew Yankowitz*

Cite This: https://doi.org/10.1021/acs.nanolett.2c02931 Read Online

ACCESS | Metrics & More | Article Recommendations | Supporting Information

ABSTRACT: The extreme versatility of van der Waals materials originates from their ability to exhibit new electronic properties when assembled in close proximity to dissimilar crystals. For example, although graphene is inherently nonmagnetic, recent work has reported a magnetic proximity effect in graphene interfaced with magnetic substrates, potentially enabling a pathway toward achieving a high-temperature quantum anomalous Hall effect. Here, we investigate heterostructures of graphene and chromium trihalide magnetic insulators (CrI_3, $CrBr_3$, and $CrCl_3$). Surprisingly, we are unable to detect a magnetic exchange field in the graphene but instead discover proximity effects featuring unprecedented gate tunability. The graphene becomes highly hole-doped due to charge transfer from the neighboring magnetic insulator and further exhibits a variety of atypical gate-dependent transport features. The charge transfer can additionally be altered upon switching the magnetic states of the nearest CrI_3 layers. Our results provide a roadmap for exploiting proximity effects arising in graphene coupled to magnetic insulators.

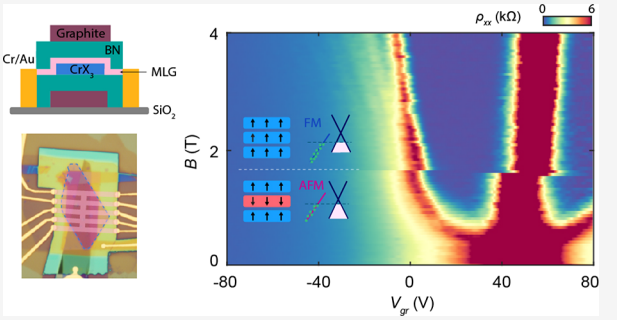

KEYWORDS: *graphene, 2D magnet, proximity effect, modulation doping, van der Waals heterostructure*

Assembling heterostructures of van der Waals (vdW) crystals enables the creation of new properties that do not exist in the constituent materials alone. For example, combining proximity-induced magnetism[1−11] and spin−orbit coupling[12−16] in graphene has been a longstanding goal, as a high-temperature quantum anomalous Hall effect is predicted to arise in such a system.[17−21] Chromium trihalides are a prototypical family of two-dimensional magnetic insulators,[22−24] and are promising for realizing a variety of proximity effects when interfaced with graphene owing to their intrinsic ferromagnetic ordering, spin−orbit coupling, and large electron affinities. However, so far pristine interfaces between graphene and chromium trihalides have not been reported owing to challenges arising from the extreme environmental sensitivity of the latter crystals.[25−27]

Here, we report low-temperature transport measurements of graphene on thin substrates of CrI_3, $CrBr_3$, and $CrCl_3$ (collectively referred to as CrX_3). Figure 1a shows a schematic of the general device structure we fabricate. Interfaces of graphene and thin CrX_3 are encapsulated with boron nitride (BN) and surrounded by top and bottom gates. The CrX_3 crystals we use range from three to tens of layers in thickness; however, a majority of our results do not appear to depend meaningfully on this parameter. In order to avoid degradation of the CrX_3 crystals during device fabrication, we first shape a flake of exfoliated graphene into a Hall bar geometry using a polymer-free anodic oxidation technique with an atomic force microscope tip[28] and then assemble the entire vdW heterostructure in an argon-filled glovebox. (See the Supporting Information and Figures S1 and S2 for full details.) We fabricate devices in which the graphene rests atop CrX_3 and vice versa, and we see the same behavior in both cases. For clarity, we henceforth refer to the bias on the gate facing the graphene (CrX_3) as V_{gr} (V_{mag}). We focus our attention primarily on graphene/CrI_3 heterostructures, from which we can additionally understand the salient properties of graphene/$CrBr_3$ and $CrCl_3$ (Supporting Information and Figures S9−S12). CrI_3 has the lowest electron affinity of the three chromium trihalides, and as a result, the modulation doping of the graphene is the smallest.

Figure 1b,c shows the resistivity of a graphene-on-trilayer CrI_3 device (device A) measured as V_{gr} (V_{mag}) is swept back

Received: July 25, 2022
Revised: September 16, 2022

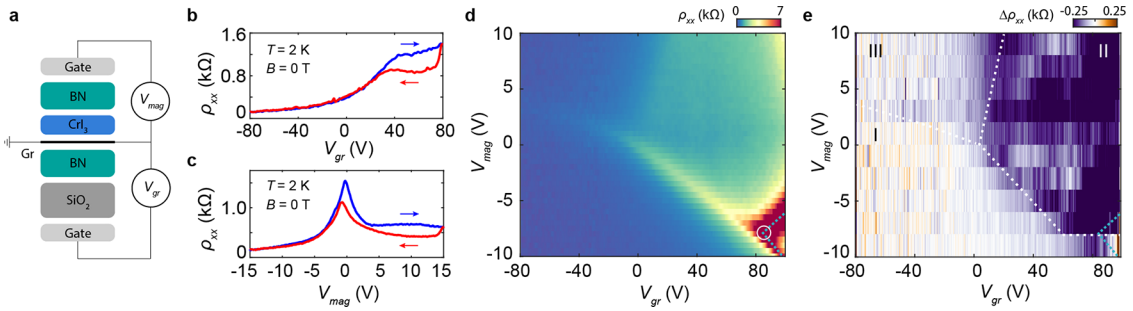

Figure 1. Transport in graphene on CrI_3 at zero magnetic field. (a) Schematic of the device structure. Monolayer graphene is interfaced with CrI_3 and encapsulated by BN. The voltage on the gate facing the graphene is V_{gr}, and the voltage on the gate facing the CrI_3 is V_{mag}. (b) Four-terminal resistivity of a device with trilayer CrI_3 (device A) as V_{gr} is swept back and forth, with $V_{mag} = 0$. (c) Resistivity as V_{mag} is swept back and forth, with $V_{gr} = 0$. (d) Map of the device resistivity acquired by sweeping both gates. The trajectory of the Dirac point is denoted by the blue dashed curve, as determined by Hall effect measurements at $B = 4$ T (Figure S3). The white circle denotes the point at which the trajectory of the Dirac point reverses. (e) Map of the transport hysteresis, $\Delta\rho_{xx}$, acquired by taking the difference between the resistivity upon slowly sweeping V_{gr} forward and backward. The white dashed curve is a guide to the eye, corresponding approximately to resistive peaks and plateaus seen in d.

and forth with the other gate grounded at a temperature of $T = 2$ K. We see a number of features that are uncharacteristic of pristine graphene encapsulated only with BN. First, the transport differs notably depending on which of the two gates is swept. Second, the transport is hysteretic, with the hysteresis most pronounced at positive values of either gate voltage. Although there are kinks or peaks in the resistivity suggestive of a Dirac point, measurements of the corresponding Hall resistance reveal that the graphene is hole-doped over most of the accessible gate voltage range (Figure S3), indicating that these resistive peaks arise from a different mechanism.

Figure 1d shows a map of the device resistivity acquired by sweeping both of the gates. The blue dashed curve traces the position of the Dirac point as determined by Hall effect measurements (Figure S3). The Dirac point evolves with the two gate voltages as anticipated from simple electrostatics in the bottom rightmost portion of the map. However, its trajectory abruptly reverses as the bias on V_{mag} is further reduced toward zero (white circle in Figure 1d). The bent trajectory of the Dirac point indicates a nonlinear and nonmonotonic relationship between the gate voltage and graphene charge carrier density, in stark contrast with the behavior of conventional monolayer graphene devices in which the gate capacitance is fixed. We see other transport features atypical of graphene, including an anomalous resistive peak that moves roughly diagonally across the map, as well as an abrupt resistive step separating the top left and right halves of the map. There is also a sharp resistivity increase in the top rightmost corner of the map that indicates the reappearance of the Dirac point. Furthermore, these features are directly associated with the hysteretic graphene transport. Figure 1e shows a measurement of $\Delta\rho_{xx}$ acquired by taking the difference between ρ_{xx} measured as V_{gr} is slowly swept back and forth (Figure S4 for the reverse measurements). As a guide to the eye, the white dashed curve denotes the positions of the anomalous resistive peak and step we observe in Figure 1d and separates the map into regions I, II, and III. The hysteresis is most prominent in region II of the map, approximately bounded by the anomalous resistive peak and step.

Transport measurements in a magnetic field, B, help to reveal the origin of these unusual features. Figure 2a,b shows Landau fan diagrams of the longitudinal, ρ_{xx} (top), and Hall, ρ_{xy} (bottom), resistivities acquired by sweeping V_{gr} from

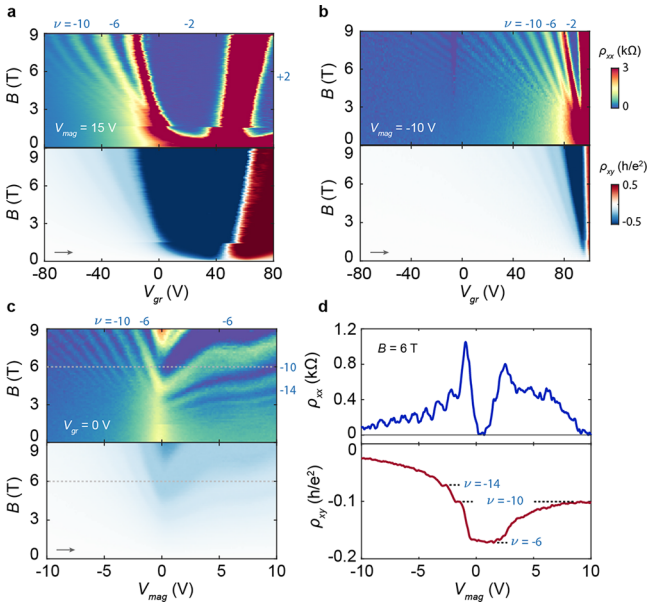

Figure 2. Landau fan diagrams of graphene on CrI_3. (a, b) (Top) Longitudinal, ρ_{xx}, and (bottom) Hall, ρ_{xy}, resistivities of device A acquired by sweeping V_{gr} from negative to positive values with (a) $V_{mag} = 15$ V and (b) $V_{mag} = -10$ V, respectively. (c) Landau fan diagram acquired by sweeping V_{mag} from negative to positive with $V_{gr} = 0$. (d) ρ_{xx} (top) and ρ_{xy} (bottom) cuts from panel c acquired at $B = 6$ T.

negative to positive bias with fixed values of $V_{mag} = 15$ V and -10 V, respectively. The latter is consistent with typical hole-doped graphene: the Dirac point appears at large positive V_{gr} and is associated with a sign change in ρ_{xy} upon doping, and there is a series of integer quantum Hall (IQH) states that disperse linearly away from the Dirac point. These correspond to filling factors of $\nu = -2, -6, -10, \ldots$, consistent with the usual sequence of states arising from spin- and valley-degenerate monolayer graphene Landau levels. In contrast, at $V_{mag} = 15$ V we see a number of anomalous features in the Landau fan, including the Dirac point drifting with magnetic field, an abrupt resistivity jump at $B = 1.6$ T, extremely wide $\nu = \pm 2$ IQH plateaus, and IQH states at higher filling factors with slightly widened plateaus that move nonlinearly.

Landau fans acquired by sweeping V_{mag} at fixed V_{gr} exhibit even more striking peculiarities. Figure 2c shows a

https://doi.org/10.1021/acs.nanolett.2c02931
Nano Lett. XXXX, XXX, XXX−XXX

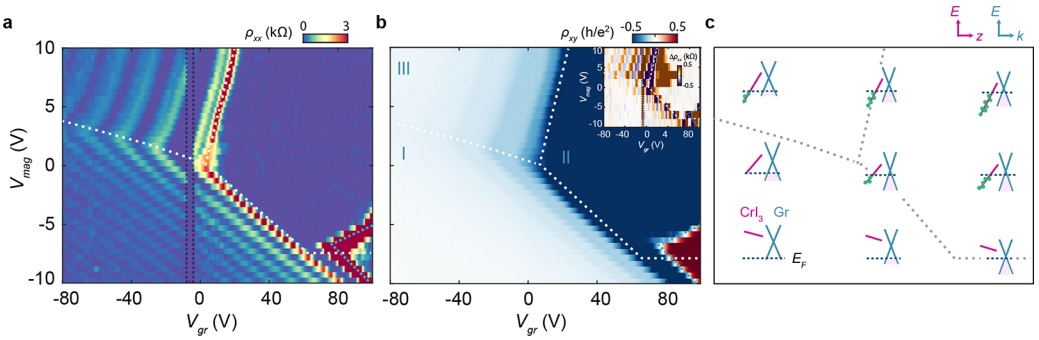

Figure 3. Mapping the charge transfer and band alignment in graphene on CrI_3. Maps of (a) ρ_{xx} and (b) ρ_{xy} acquired by sweeping both gates at B = 9 T. The white dotted lines are the same guides to the eye as in Figure 1e and separate the map into regions I−III. The ν = 0 state, corresponding to the Dirac point, is determined by the sign change in ρ_{xy} (blue dashed curve). (Inset of b) Map of the transport hysteresis, $\Delta\rho_{xx}$, acquired at B = 9 T. The regions enclosed within the vertical black and gray boxes in panel a and the inset of panel b are contaminated by artifacts owing to insulating behavior at the contacts. (c) Inferred alignment of the graphene Dirac cone (blue) and the lowest electron-holding states in CrI_3 (red) under different gating conditions, corresponding to the approximate corresponding positions from the maps in panels a and b. Because CrI_3 is multiple layers thick, gate voltages establish an electric field across the sheet which tilts the bands. The band offset at the interface between the graphene and adjacent CrI_3 layer is a fixed quantity determined by the graphene work function and CrI_3 electron affinity. The dark-blue dashed line denotes the Fermi energy, E_F, in the graphene. Filled states in graphene are indicated in pink, and electrons in CrI_3 are denoted schematically by the green dots. The axes on the top right are color coded; the vertical denotes energy for both, whereas the horizontal denotes momentum for the graphene and c-axis position for the few-layer CrI_3.

representative example in which the IQH states disperse as expected for $V_{mag} \lesssim 0$ but abruptly reverse direction for $V_{mag} \gtrsim 0$. The latter regime corresponds to an apparent negative compressibility of the system in which applying a more positive gate voltage results in filling additional hole-type Landau levels rather than their anticipated depletion. Figure 2d shows a representative example of this phenomenon at B = 6 T in which the graphene exhibits two disconnected regimes of doping corresponding to the ν = −10 IQH state.

The IQH states in typical graphene devices fan out linearly from the Dirac point as the magnetic field is raised. Their trajectories are described by the Středa formula,[29] $\nu = (h/e)(\partial n/\partial B)$, where h is Planck's constant, e is the charge of the electron, and n is the charge carrier density. Departure from this behavior provides further evidence of the nonlinear relationship between the gate voltage and the charge carrier density in the graphene originating from the charge transfer with the CrI_3, consistent with the bent trajectory of the Dirac point observed in Figure 1d. The wide IQH plateaus and their nonlinear trajectories in the fan diagram indicate that the charges induced by the gate do not accumulate in the graphene but rather fill the CrI_3 since electrons become localized in the insulating CrI_3 and do not contribute to transport. Related effects have been previously observed in graphene on SiC[30−34] and CrOCl.[35] The coexistence of normal and atypical quantum Hall effects within our device suggests that the modulation doping can be controlled by gating and under suitable conditions is even suppressed entirely.

We characterize the full dependence of the charge transfer on the gating and magnetic field by measuring ρ_{xx} and ρ_{xy} over the entire accessible range of both gate voltages at a fixed B = 9 T (Figure 3a,b). For the purposes of analyzing the behavior, we divide the map into three regions as marked by the white dotted lines (reproduced from Figure 1e). region I exhibits typical graphene magnetotransport in which a sequence of hole-doped IQH states is dispersed diagonally. The negative slope of these features is consistent with the ratio of the geometrical capacitances of the top and bottom gates. This remains true for the ν = 0 insulating state in the bottom right corner of the map, across which the sign of the Hall effect flips. In contrast, region II corresponds almost entirely to the ν = −2 IQH state. At the foot of region II, we observe an abrupt reversal in the trajectory of the ν = 0 state similar to that of the Dirac point at B = 0 (Figure 1d). In region III, the IQH states become nearly insensitive to V_{mag} and develop a positive slope. The inset of Figure 3b shows hysteresis measurements, $\Delta\rho_{xx}$, acquired at B = 9 T, analogous to the zero-field map shown in Figure 1e. The hysteresis is primarily confined to region III; however, we note that this measurement scheme is largely insensitive to the hysteresis in region II owing to the extended ν = −2 plateau. In combination with the zero-field measurements (Figure 1e), we deduce that the device exhibits hysteresis in both regions II and III. The hysteresis is therefore directly associated with regions of atypical graphene transport and does not occur in region I where the transport is conventional.

The above measurements can all be qualitatively understood by taking into account the gate- and field-dependent charge density in the CrI_3. Figure 3c shows a series of cartoon diagrams that depict the electron states and their occupancies in the graphene (blue) and CrI_3 (red) for different combinations of the top and bottom gate voltages. Filled states in graphene below the chemical potential (blue dashed line) are colored pink. The red line represents the lowest-energy electron states in the CrI_3 and corresponds either to the bottom of the conduction band or to a band of in-gap defect states; the latter is more likely because the charge mobility is very low. Electrons in the CrI_3 are indicated by the green dots. We assume that the alignment between the graphene Dirac point and the lowest-energy electron band in the neighboring CrI_3 layer is fixed by the combination of the graphene work function and CrI_3 electron affinity. Biasing V_{mag} establishes an electric field across the few-layer CrI_3, shifting the energy of the CrI_3 states either up or down relative to the graphene.

Within region I, the chemical potential lies beneath the lowest-energy electron states throughout the CrI_3, and as a result, they are all unoccupied. The CrI_3 then simply behaves as a dielectric, and changing the bias on either gate capacitively dopes the graphene as usual. In regions II and III, the bias V_{mag} is such that some electron states in the CrI_3 are below the

https://doi.org/10.1021/acs.nanolett.2c02931
Nano Lett. XXXX, XXX, XXX−XXX

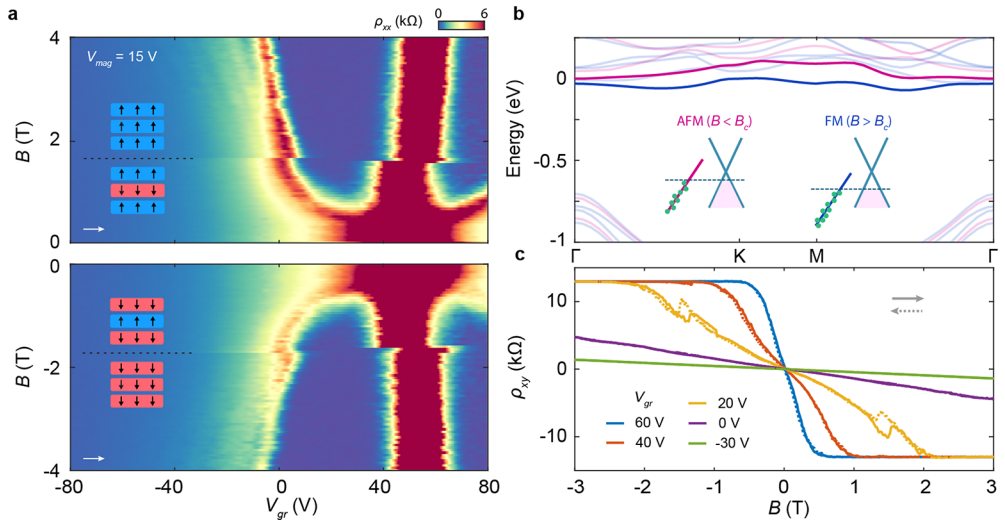

Figure 4. Magnetic field-dependent modulation doping of graphene on CrI_3. (a) Low-field Landau fan diagram acquired by sweeping V_{gr} from negative to positive with V_{mag} = 15 V. An abrupt shift in the modulation doping is denoted by the black dashed line, corresponding to the critical field at which the trilayer CrI_3 flips between interlayer AFM and FM (illustrated by the cartoon insets). (b) Ab initio calculation of the band structure of bilayer CrI_3 in the interlayer FM (blue) and AFM (red) states. The lowest conduction band is highlighted for clarity. The cartoon illustrates the additional modulation doping of graphene anticipated in the FM state compared with the AFM state owing to the lower conduction band energy. (c) ρ_{xy} acquired by sweeping B back and forth at different values of V_{gr}, with V_{mag} = 15 V.

chemical potential, causing electrons to tunnel into them from the graphene. These electrons become almost entirely localized and contribute negligibly to the conductivity but are mobile enough in the out-of-plane direction to screen the underlying gate. This results in a greatly altered sensitivity of the graphene doping to changes in V_{mag}. The hysteresis observed in these regions results from an inability of the electrons to reach a true equilibrium due to long time scales in the CrI_3. As further evidence for this, we observe irreversible changes in the modulation-doping of the graphene in measurements performed days apart (Figure S14), and in a graphene/$CrCl_3$ device doped to a similar regime, the resistance exhibits telegraph noise on a time scale of tens of minutes when both gate voltages are held fixed (Figure S15).

The distinction between regions II and III can be explained by the density of states in the graphene, which is small or vanishing in the former and much larger in the latter. These regions are separated by a resistivity plateau at zero field and by a crossover at 9 T from the highly extended $\nu = -2$ IQH plateau to a sequence of less extended IQH states with higher filling factors. In region II, changes in V_{mag} are almost entirely screened. In this region, changing V_{gr} only weakly dopes the graphene because the low density of states means that adding electrons to the graphene causes its electrochemical potential to rise rapidly, leading to more electrons tunneling into the CrI_3. In region III, changing V_{gr} dopes the graphene more strongly because its density of states is larger. Meanwhile, changing V_{mag} does dope the graphene somewhat, but, strikingly, it does so in the wrong sense. In this case, the IQH states have positive slope indicative of an effectively negative differential capacitance. In other words, a more positive V_{mag} results in larger hole doping of the graphene, whereas naively it would be expected to instead reduce the hole doping. This effect is also responsible for the peculiar reversal of the trajectories of the IQH plateaus seen near V_{mag} = 0 in the Landau fans shown in Figure 2c,d. Negative differential capacitance can result from negative compressibility in a strongly correlated conductor, such as has been reported for graphene on MoS_2.[36] It can also result from a large rearrangement of charge in the dielectric induced by a small change in the applied electric field, such as occurs when a ferroelectric polarization flips. Rearrangement of the interacting electrons within the CrI_3 therefore seems to be the most likely explanation for this phenomenon and is consistent with the associated hysteresis, though it appears to be too complex to be usefully modeled at this point.

So far, we have not considered the role of the magnetic ordering of the CrI_3, which exhibits out-of-plane intralayer ferromagnetism (FM) and antiferromagnet (AFM) interlayer ordering at low temperature. Figure 4a shows a low-field Landau fan diagram acquired for both positive and negative values of B. As noted earlier, upon increasing the field there is an abrupt jump close to $|B| = 1.6$ T at which all resistance features shift toward more positive V_{gr}, indicating a sudden transfer of electrons out of the graphene. To interpret this, we consider a simple model in which the CrI_3 is a bilayer in order to investigate the origin of this effect, justified by the expectation that the graphene couples most strongly to the nearest few layers of the CrI_3. Ab initio calculations show that the energy of the CrI_3 conduction band depends on its interlayer magnetic ordering, shifting to lower energy as the material undergoes a transition from interlayer AFM to FM (Figure 4b). This transition likely also reduces the energy levels of defect states and results in additional electrons tunneling into the CrI_3. (See the band schematics in Figure 4b.) This abrupt jump is absent in region I, where the states in the CrI_3 remain too high to be occupied (e.g., see Figure 2b). This effect demonstrates that the graphene resistivity is highly sensitive to the interlayer magnetic ordering of the CrI_3. We find that the critical field becomes asymmetric with the sweeping direction of the magnetic field for thicker CrI_3 substrates (Figure S18), indicating that the graphene is only sensitive to the magnetic ordering of the nearest few CrI_3 layers.

The anomalous Hall effect (AHE) is anticipated in graphene endowed with both a magnetic exchange field and Rasbha spin

https://doi.org/10.1021/acs.nanolett.2c02931
Nano Lett. XXXX, XXX, XXX−XXX

orbit coupling,[17−21] owing to the formation of an inverted gap at the Dirac point and associated Berry curvature at the band edges. We search for the AHE by measuring ρ_{xy} as the magnetic field is swept back and forth at different values of V_{gr} (Figure 4c). We see hysteretic loops surrounding $|B| \approx 1.6$ T owing to the AFM/FM transition in the CrI_3 but do not observe hysteresis at $B = 0$. For measurements acquired near the Dirac point, we observe nonlinear $\rho_{xy}(B)$ surrounding $B = 0$ reminiscent of a weak AHE. However, we also notice that the Dirac point drifts with magnetic field in the Landau fans shown in Figures 2a and 4a. Although we do not understand the origin of this effect and further find that it is highly sample-dependent (e.g., see Figure S5f), its presence here implies that the charge transfer between the graphene and CrI_3 changes continuously with the magnetic field. As a result, the charge carrier density in graphene also changes with B at fixed gate voltage, potentially driving a nonlinearity in the observed Hall effect that is completely unrelated to the usual AHE mechanism.

Careful analysis of the Landau fans can provide further insights into the strength of the magnetic proximity coupling in graphene. As detailed earlier, we observe a 4-fold degeneracy in nearly all of the IQH states in our sample (with only weak signatures of symmetry breaking at high B), indicating preserved spin and valley degeneracy. The absence of symmetry-broken IQH states is expected given the modest graphene mobility of ∼5000 $cm^2/(V\ s)$ (Figure S19), presumably resulting from scattering due to defects in the CrI_3 substrate. However, the absence of detectable Landau-level splitting also sets an upper bound on the magnitude of the magnetic exchange coupling, which is expected to act as a Zeeman term that lifts the spin degeneracy at zero field. The magnetic exchange coupling must therefore be less than the smallest resolvable Landau-level gap in our measurements. We estimate this to be ∼25 meV from the fact that the $\nu = -2$ state fully develops at $B \approx 0.5$ T (Figure 4c), following the expectation that the corresponding cyclotron gap is $\Delta E_{-2} = v_F\sqrt{2\hbar eB}$, where $v_F = 10^6$ m/s is the presumed Fermi velocity of graphene and $\hbar$ is Planck's reduced constant. This is in tension with theoretical predictions of magnetic exchange couplings ranging from tens of meV to as large as ∼120 meV in graphene on CrI_3.[37−39] Furthermore, unambiguous evidence for a proximity exchange field has been observed in optical spectroscopy measurements of monolayer WSe_2 on a CrI_3 substrate.[40,41] The apparent unexpectedly small exchange coupling for graphene on CrI_3 may be intrinsic, but it may also be degraded by disorder in the CrI_3 for reasons that are not clear at present. Progress toward a high-temperature quantum anomalous Hall effect in proximitized graphene will likely require a reduction of the defect concentration in the CrI_3 crystal or the discovery of more favorable magnetic insulator substrates.

■ ASSOCIATED CONTENT

Supporting Information

The Supporting Information is available free of charge at https://pubs.acs.org/doi/10.1021/acs.nanolett.2c02931.

Experimental methods; summary of devices; details of the device fabrication; determination of the Dirac point position; additional transport data for the device presented in the main text; transport data from additional graphene/CrI_3 devices, graphene/$CrBr_3$, and $CrCl_3$ devices; temperature-dependent transport; characterization of hysteresis; transport in a device with a monolayer WSe_2 spacer; sensing the magnetic ordering of the CrI_3; and determination of the graphene mobility (PDF)

■ AUTHOR INFORMATION

Corresponding Author

Matthew Yankowitz − *Department of Physics and Department of Materials Science and Engineering, University of Washington, Seattle, Washington 98195, United States;* orcid.org/0000-0002-5637-9203; Email: myank@uw.edu

Authors

Chun-Chih Tseng − *Department of Physics, University of Washington, Seattle, Washington 98195, United States;* Present Address: C.-C.T. and T.S. contributed equally to this work

Tiancheng Song − *Department of Physics, University of Washington, Seattle, Washington 98195, United States;* Present Address: C.-C.T. and T.S. contributed equally to this work; orcid.org/0000-0002-6845-6624

Qianni Jiang − *Department of Physics, University of Washington, Seattle, Washington 98195, United States*

Zhong Lin − *Department of Physics, University of Washington, Seattle, Washington 98195, United States;* orcid.org/0000-0001-9505-5538

Chong Wang − *Department of Materials Science and Engineering, University of Washington, Seattle, Washington 98195, United States*

Jaehyun Suh − *Department of Materials Science and Engineering, University of Washington, Seattle, Washington 98195, United States*

Kenji Watanabe − *Research Center for Functional Materials, National Institute for Materials Science, Tsukuba 305-0044, Japan;* orcid.org/0000-0003-3701-8119

Takashi Taniguchi − *International Center for Materials Nanoarchitectonics, National Institute for Materials Science, Tsukuba 305-0044, Japan;* orcid.org/0000-0002-1467-3105

Michael A. McGuire − *Materials Science and Technology Division, Oak Ridge National Laboratory, Oak Ridge, Tennessee 37831, United States;* orcid.org/0000-0003-1762-9406

Di Xiao − *Department of Physics and Department of Materials Science and Engineering, University of Washington, Seattle, Washington 98195, United States; Pacific Northwest National Laboratory, Richland, Washington 99354, United States*

Jiun-Haw Chu − *Department of Physics, University of Washington, Seattle, Washington 98195, United States*

David H. Cobden − *Department of Physics, University of Washington, Seattle, Washington 98195, United States*

Xiaodong Xu − *Department of Physics and Department of Materials Science and Engineering, University of Washington, Seattle, Washington 98195, United States;* orcid.org/0000-0003-0348-2095

Complete contact information is available at: https://pubs.acs.org/10.1021/acs.nanolett.2c02931

https://doi.org/10.1021/acs.nanolett.2c02931
Nano Lett. XXXX, XXX, XXX−XXX

Author Contributions

C.-C.T. and T.S. fabricated the devices, with assistance from J.S. C.-C.T. and T.S. performed the measurements. Q.J., Z.L., and J.-H.C. provided the bulk CrI_3 and $CrBr_3$ crystals. M.A.M. provided the bulk $CrCl_3$ crystals. K.W. and T.T. provided the bulk BN crystals. C.W. and D.X. calculated the CrI_3 band structure. C.-C.T. and T.S. analyzed the data under the supervision of D.H.C., X.X., and M.Y.

Notes

The authors declare no competing financial interest.

■ ACKNOWLEDGMENTS

This work was supported as part of Programmable Quantum Materials, an Energy Frontier Research Center funded by the U.S. Department of Energy (DOE), Office of Science, Basic Energy Sciences (BES), under award DE-SC0019443. M.Y., X.X., and J.-H.C. acknowledge support from the State of Washington-funded Clean Energy Institute. This work made use of shared fabrication facilities provided by NSF MRSEC 1719797. The material synthesis at UW is partially supported by the Gordon and Betty Moore Foundation's EPiQS Initiative, Grant GBMF6759 to J.-H.C. K.W. and T.T. acknowledge support from the Elemental Strategy Initiative conducted by the MEXT, Japan (grant number JPMXP0112101001) and JSPS KAKENHI (grant numbers 19H05790, 20H00354, and 21H05233). M.A.M.'s crystal synthesis effort at ORNL was supported by the U.S. Department of Energy, Office of Science, Basic Energy Sciences, Materials Sciences and Engineering Division.

■ REFERENCES

(1) Wang, Z.; Tang, C.; Sachs, R.; Barlas, Y.; Shi, J. Proximity-induced ferromagnetism in graphene revealed by the anomalous Hall effect. *Phys. Rev. Lett.* **2015**, *114*, 016603.

(2) Wei, P.; Lee, S.; Lemaitre, F.; Pinel, L.; Cutaia, D.; Cha, W.; Katmis, F.; Zhu, Y.; Heiman, D.; Hone, J.; S, M. J.; Chen, C.-T. Strong interfacial exchange field in the graphene/EuS heterostructure. *Nat. Mater.* **2016**, *15*, 711−716.

(3) Leutenantsmeyer, J. C.; Kaverzin, A. A.; Wojtaszek, M.; van Wees, B. J. Proximity induced room temperature ferromagnetism in graphene probed with spin currents. *2D Materials* **2017**, *4*, 014001.

(4) Xu, J.; Singh, S.; Katoch, J.; Wu, G.; Zhu, T.; uti, I.; Kawakami, R. K. Spin inversion in graphene spin valves by gate-tunable magnetic proximity effect at one-dimensional contacts. *Nat. Commun.* **2018**, *9*, 2869.

(5) Tang, C.; Cheng, B.; Aldosary, M.; Wang, Z.; Jiang, Z.; Watanabe, K.; Taniguchi, T.; Bockrath, M.; Shi, J. Approaching quantum anomalous Hall effect in proximity-coupled YIG/graphene/h-BN sandwich structure. *APL Materials* **2018**, *6*, 026401.

(6) Karpiak, B.; Cummings, A. W.; Zollner, K.; Vila, M.; Khokhriakov, D.; Hoque, A. M.; Dankert, A.; Svedlindh, P.; Fabian, J.; Roche, S. Magnetic proximity in a van der Waals heterostructure of magnetic insulator and graphene. *2D Materials* **2020**, *7*, 015026.

(7) Tang, C.; Zhang, Z.; Lai, S.; Tan, Q.; Gao, W.-B. Magnetic proximity effect in graphene/$CrBr_3$ van der Waals heterostructures. *Adv. Mater.* **2020**, *32*, 1908498.

(8) Wu, Y.; Yin, G.; Pan, L.; Grutter, A. J.; Pan, Q.; Lee, A.; Gilbert, D. A.; Borchers, J. A.; Ratcliff, W., II; Li, A.; Han, X.-D.; Wang, K. L. Large exchange splitting in monolayer graphene magnetized by an antiferromagnet. *Nature Electronics* **2020**, *3*, 604−611.

(9) Ghiasi, T. S.; Kaverzin, A. A.; Dismukes, A. H.; de Wal, D. K.; Roy, X.; van Wees, B. J. Electrical and thermal generation of spin currents by magnetic bilayer graphene. *Nat. Nanotechnol.* **2021**, *16*, 788−794.

(10) Wu, Y.; Cui, Q.; Zhu, m.; Liu, X.; Wang, Y.; Zhang, J.; Zheng, X.; Shen, J.; Cui, P.; Yang, H.; Wang, S. Magnetic Exchange Field Modulation of Quantum Hall Ferromagnetism in 2D van der Waals $CrCl_3$/Graphene Heterostructures. *ACS Appl. Mater. Interfaces* **2021**, *13*, 10656−10663.

(11) Chau, T. K.; Hong, S. J.; Kang, H.; Suh, D. Two-dimensional ferromagnetism detected by proximity-coupled quantum Hall effect of graphene. *npj Quantum Materials* **2022**, *7*, 27.

(12) Avsar, A.; Tan, J. Y.; Taychatanapat, T.; Balakrishnan, J.; Koon, G. K. W.; Yeo, Y.; Lahiri, J.; Carvalho, A.; Rodin, A. S.; OFarrell, E. C. T.; Eda, G.; Castro Neto, A. H.; zyilmaz, B. Spinorbit proximity effect in graphene. *Nat. Commun.* **2014**, *5*, 4875.

(13) Wang, Z.; Ki, D.-K.; Chen, H.; Berger, H.; MacDonald, A. H.; Morpurgo, A. F. Strong interface-induced spin-orbit interaction in graphene on WS_2. *Nat. Commun.* **2015**, *6*, 8339.

(14) Wang, Z.; Ki, D.-K.; Khoo, J. Y.; Mauro, D.; Berger, H.; S, L. L.; Morpurgo, A. F. Origin and magnitude of designer spin-orbit interaction in graphene on semiconducting transition metal dichalcogenides. *Physical Review X* **2016**, *6*, 041020.

(15) Yang, B.; Tu, M.-F.; Kim, J.; Wu, Y.; Wang, H.; Alicea, J.; Wu, R.; Bockrath, M.; Shi, J. Tunable spin-orbit coupling and symmetry-protected edge states in graphene/WS2. *2D Materials* **2016**, *3*, 031012.

(16) Island, J. O.; Cui, X.; Lewandowski, C.; Khoo, J. Y.; Spanton, E. M.; Zhou, H.; Rhodes, D.; Hone, J. C.; Taniguchi, T.; Watanabe, K.; Levitov, L. S.; Zaletel, M. P.; Young, A. F. Spin-orbit-driven band inversion in bilayer graphene by the van der Waals proximity effect. *Nature* **2019**, *571*, 85−89.

(17) Qiao, Z.; Yang, S. A.; Feng, W.; Tse, W.-K.; Ding, J.; Yao, Y.; Wang, J.; Niu, Q. Quantum anomalous Hall effect in graphene from Rashba and exchange effects. *Phys. Rev. B* **2010**, *82*, 161414.

(18) Qiao, Z.; Ren, W.; Chen, H.; Bellaiche, L.; Zhang, Z.; MacDonald, A. H.; Niu, Q. Quantum anomalous Hall effect in graphene proximity coupled to an antiferromagnetic insulator. *Phys. Rev. Lett.* **2014**, *112*, 116404.

(19) Zhang, J.; Zhao, B.; Yao, Y.; Yang, Z. Robust quantum anomalous Hall effect in graphene-based van der Waals heterostructures. *Phys. Rev. B* **2015**, *92*, 165418.

(20) Zhang, J.; Zhao, B.; Zhou, T.; Xue, Y.; Ma, C.; Yang, Z. Strong magnetization and Chern insulators in compressed graphene/CrI_3 van der Waals heterostructures. *Phys. Rev. B* **2018**, *97*, 085401.

(21) Hg, P.; Frank, T.; Zollner, K.; Kochan, D.; Gmitra, M.; Fabian, J. Quantum anomalous Hall effects in graphene from proximity-induced uniform and staggered spin-orbit and exchange coupling. *Phys. Rev. B* **2020**, *124*, 136403.

(22) Huang, B.; Clark, G.; Navrro-Moratalla, E.; Klein, D. R.; Cheng, R.; Seyler, K. L.; Zhong, D.; Schmidgall, E.; McGuire, M. A.; Cobden, D. H.; Yao, W.; Xiao, D.; Jarillo-Herrero, P.; Xu, X. Layer-dependent ferromagnetism in a van der Waals crystal down to the monolayer limit. *Nature* **2017**, *546*, 270−273.

(23) Zhang, Z.; Shang, J.; Jiang, C.; Rasmita, A.; Gao, W.; Yu, T. Direct photoluminescence probing of ferromagnetism in monolayer two-dimensional $CrBr_3$. *Nano Lett.* **2019**, *19*, 3138−3142.

(24) Cai, X.; Song, T.; Wilson, N. P.; Clark, G.; He, M.; Zhang, X.; Taniguchi, T.; Watanabe, K.; Yao, W.; Xiao, D.; McGuire, M. A.; Cobden, D. H.; Xu, X. Atomically thin $CrCl_3$: an in-plane layered antiferromagnetic insulator. *Nano Lett.* **2019**, *19*, 3993−3998.

(25) Shcherbakov, D.; Stepanov, P.; Weber, D.; Wang, Y.; Hu, J.; Watanabe, K.; Taniguchi, T.; Mao, Z.; Windl, W.; Goldberger, J.; Bockrath, M.; Lau, C. N. Raman Spectroscopy, Photocatalytic Degradation, and Stabilization of Atomically Thin Chromium Triiodide. *Nano Lett.* **2018**, *18*, 4214−4219.

(26) Wang, Z.; Gutirrez-Lezama, I.; Ubrig, N.; Kroner, M.; Gibertini, M.; Taniguchi, T.; Watanabe, K.; Imamolu, A.; Giannini, E.; Morpurgo, A. F. Very Large Tunneling Magnetoresistance in Layered Magnetic Semiconductor CrI_3. *Nat. Commun.* **2018**, *9*, 2516.

(27) Gish, J. T.; Lebedev, D.; K, S. T.; Jiang, S.; Georgopoulos, L.; Dong, T. W.; Lim, G.; Garvey, E. S.; Valdman, L.; Balogun, O.; Sofer, Z.; Sangwan, N. P.; Stern, V. K.; Hersam, M. C. Ambient-Stable Two-Dimensional CrI_3 via Organic-Inorganic Encapsulation. *ACS Nano* **2021**, *15*, 10659−10667.

https://doi.org/10.1021/acs.nanolett.2c02931
Nano Lett. XXXX, XXX, XXX−XXX

(28) Li, H.; Ying, Z.; Lyu, B.; Deng, A.; Wang, L.; Taniguchi, T.; Watanabe, K.; Shi, Z. Electrode-Free Anodic Oxidation Nanolithography of Low-Dimensional Materials. *Nano Lett.* **2018**, *18*, 8011−8015.
(29) Streda, P. Quantised Hall effect in a two-dimensional periodic potential. *Journal of Physics C: Solid State Physics* **1982**, *15*, L1299.
(30) Tzalenchuk, A.; Lara-Avila, S.; Kalaboukhov, A.; Paolillo, S.; Syvjrvi, M.; Yakimova, R.; Kazakova, O.; Janssen, T. J. B. M.; Fal'ko, V.; Kubatkin, S. Towards a quantum resistance standard based on epitaxial graphene. *Nat. Nanotechnol.* **2010**, *5*, 186−189.
(31) Janssen, T. J. B. M.; Tzalenchuk, A.; Yakimova, R.; Kubatkin, S.; Lara-Avila, S.; Kopylov, S.; Fal'ko, V. Anomalously strong pinning of the filling factor $\nu = 2$ in epitaxial graphene. *Phys. Rev. B* **2011**, *83*, 233402.
(32) Janssen, T. J. B. M.; Tzalenchuk, A.; Kubatkin, S.; Lara-Avila, S.; Kopylov, S.; Fal'ko, V. Quantum resistance metrology using graphene. *Rep. Prog. Phys.* **2013**, *76*, 104501.
(33) Lafont, F.; Ribeiro-Palau, R.; Kazazis, D.; Michon, A.; Couturaud, O.; Consejo, C.; Chassagne, T.; Zielinski, M.; Portail, M.; Jouault, B.; Schopfer, F.; W, P. Quantum Hall resistance standards from graphene grown by chemical vapour deposition on silicon carbide. *Nat. Commun.* **2015**, *6*, 6806.
(34) Alexander-Webber, J. A.; Huang, J.; Maude, D. K.; Janssen, T. J. B.; Tzalenchuk, A.; Antonov, V.; Yager, T.; Lara-Avila, S.; Yakimova, R.; Nicholas, R. J. Giant quantum Hall plateaus generated by charge transfer in epitaxial graphene. *Sci. Rep.* **2016**, *6*, 30296.
(35) Wang, Y.; Gao, X.; Yang, K.; Gu, P.; Dong, B.; Jiang, Y.; Watanabe, K.; Taniguchi, T.; Kang, J.; Lou, W.; Mao, J.; Ye, Y.; Han, Z. V.; Chang, K.; Zhang, J.; Zhang, Z.*Flavoured quantum Hall phase in graphene/CrOCl heterostructures*; arXiv:2110.02899, 2021 (accessed July 25, 2022).
(36) Larentis, S.; Tolsma, J. R.; Fallahazad, B.; Dillen, D. C.; Kim, K.; MacDonald, A. H.; Tutuc, E. Band Offset and Negative Compressibility in Graphene-MoS2 Heterostructures. *Nano Lett.* **2014**, *14*, 2039−2045.
(37) Holmes, A. M.; Pakniyat, S.; Gangaraj, S. A. H.; Monticone, F.; M, W.; Hanson, G. W. Exchange splitting and exchange-induced nonreciprocal photonic behavior of graphene in CrI_3-graphene van der Waals heterostructures. *Phys. Rev. B* **2020**, *102*, 075435.
(38) Farooq, M. U.; Hong, J. Switchable valley splitting by external electric field effect in graphene/CrI_3 heterostructures. *npj 2D Materials and Applications* **2019**, *3*, 33.
(39) Zhang, J.; Zhao, B.; Zhou, T.; Xue, Y.; Ma, C.; Yang, Z. Strong magnetization and Chern insulators in compressed graphene/CrI_3 van der Waals heterostructures. *Phys. Rev. B* **2018**, *97*, 085401.
(40) Zhong, K. L.; Seyler, D.; Linpeng, X.; Cheng, R.; Sivadas, N.; Huang, B.; Schmidgall, E.; Taniguchi, T.; Watanabe, K.; McGuire, M. A.; Yao, W.; Xiao, D.; Fu, K.-M. C.; Xu, X. Van der Waals engineering of ferromagnetic semiconductor heterostructures for spin and valleytronics. *Science Advances* **2017**, *3*, e1603113.
(41) Zhong, D.; Seyler, K. L.; Linpeng, X.; Wilson, N. P.; Taniguchi, T.; Watanabe, K.; McGuire, M. A.; Fu, K.-M. C.; Xiao, D.; Yao, W.; Xu, X. Layer-resolved magnetic proximity effect in van der Waals heterostructures. *Nat. Nanotechnol.* **2020**, *15*, 187−191.

https://doi.org/10.1021/acs.nanolett.2c02931
Nano Lett. XXXX, XXX, XXX−XXX